Hindawi
International Journal of Antennas and Propagation
Volume 2018, Article ID 8962048, 12 pages
https://doi.org/10.1155/2018/8962048

Research Article

Stepped Frequency Pulse Frequency Diverse Array Radar for Target Localization in Angle and Range Domains

Ming Tan, Chun-yang Wang, Zhi-hui Li, Xin Li, and Lei Bao

Air and Missile Defense College of Air Force Engineering University, Xi'an, Shanxi 710051, China

Correspondence should be addressed to Ming Tan; tanming_1992@163.com

Received 13 June 2018; Accepted 8 August 2018; Published 12 September 2018

Academic Editor: Andrea Francesco Morabito

Unlike phased array bringing angle-dependent and range-independent beamforming, a new kind of radar system called frequency diverse array (FDA) has been widely used for its ability to generate angle-range-dependent beampattern, which provides a broad prospect of radar application. Nevertheless, FDA beampattern is coupling in the angle and range responses, which results in the difficulty for FDA to differentiate the target in two domains simultaneously. In this paper, a stepped frequency pulse FDA (SFP-FDA) radar is proposed to wipe off the angle-range coupling in FDA and improve the target's angle and range localization accuracy. Compared to the double-pulse FDA, the proposed system can achieve a better performance in range resolution and multitarget identification. The Cramér-Rao lower bound (CRLB) is derived and used to analyze the performance of the proposed system and double-pulse FDA radar. Numerical results are implemented to verify the validity of the proposed scheme.

1. Introduction

Target localization is to find a way to calculate the position parameters of the target, and the angle and range parameters do draw much attention in localization [1]. The phased array radar [2, 3] has been widely employed for its capability to orientate the direction of the target [4, 5]. Due to its range ambiguity [6], phased array radar cannot distinguish targets from different ranges in a particular angle. To address the current needs for controlling range-dependent transmit energy distribution, a more agile array radar called frequency diverse array (FDA) radar is put forward by Antonik et al. [7–9]. By using a tiny frequency offset among antenna elements, FDA can achieve an angle-range-dependent beamforming [10]. The degree of freedom is increased, and this bidimensional property can be widely utilized, such as interference rejection [11], moving target indication [12], range ambiguity resolution, and target localization [13, 14].

Because of its wide application prospects, FDA has attracted extensive attention in recent years [15–18]. A technology for FDA antenna systems that could generate angle-range-dependent beamforming is put forward in [19]. The multipath features of FDA on the ground propagation are studied in [20]. The Cramér-Rao lower bounds (CRLBs) of FDA for estimating range, angle, and velocity are derived in [21]. Some researchers are trying to find a transmit beampattern, which can last for a period of time in focusing signal power on the expected location [22]. A FDA structure based on periodic triangular frequency-modulated continuous waveform is put forward in [23]. To realize low probability of intercept, the cognitive FDA MIMO radar is presented in [24]. Global optimization algorithm like genetic algorithm is discussed to generate a thumbtack-shaped beampattern [25]. A multicarrier nonlinear frequency modulation FDA system based on pseudorandom frequency offset is presented in [26]. The system is simplified by omitting the optimization algorithm, and signal power can focus on different targets during desired time period. To attain a required radiation performance, such as the element placements and frequency offsets, the sparse FDA technology based on artificial bee colony optimizer is proposed in [27]. A new beampattern synthesis method for FDA radar is presented in [28], which incorporating an arc-tangent function-modulated frequency scheme.

The target angles and ranges are jointly estimated by the MUSIC method in [29]. A multitarget localization algorithm, which incorporating the coprime arrays and the coprime frequency increments for the sparse FDA radar, is proposed in [14]. To realize unambiguous frequency pattern identification, a simple criterion derived by an eigenvector-based method for target localization is presented in [30]. Unlike [14, 29, 30], a concept of double-pulse FDA radar with frequency increments being zero and nonzero is presented in [31] to achieve the target localization. Two steps are needed in this method to estimate the angle and range, respectively. In the first step, a zero frequency increment FDA, i.e., phased array, is utilized to estimate the target in the angle dimension. Then, the angle information is used as the prior knowledge and the range of the target is localized by another pulse with nonzero frequency increment.

In this paper, we propose a FDA transmit scheme called stepped frequency pulse FDA (SFP-FDA). In the proposed scheme, the SFP-FDA radar, like FDA radar, radiating a signal with a bit of frequency increment between the array elements in the first pulse, the difference is that there is another frequency interval between adjacent pulses. Due to the angle and range coupling of the beampattern, both the two dimensions of target cannot be estimated by FDA radar directly. Hence, the double-pulse FDA [31] which aims at angle-range localization of targets is proposed. The proposed system in this paper can be regarded as a kind of transformation or upgrading of [31], taking part of the amount of computation as a cost. It performs better in range resolution and multitarget localization. The data model and beamforming principle have been derived. The CRLB estimation of the proposed radar and the double-pulse radar are derived and simulated. And their performances are compared and analyzed.

The remaining sections are organized as follows. Section 2 gives some important details about FDA radar and phased array radar. Section 3 presents the mathematical principle and design technique of SFP-FDA radar. The SFP-FDA radar's data model and the details of the targets' localization in angle and range domains are proposed in Section 4. Section 5 derives the CRLB estimation performance. Next, Section 6 provides the numerical results and discussions. Finally, the conclusion is drawn in Section 7.

2. Frequency Diverse Array and Phased Array Radar

Consider the case where the frequency fed to nth element of an N element uniform linear array is [7–10].

$$f_n = f_0 + n\Delta f_a \quad n = 0, 1, \ldots, N-1, \tag{1}$$

where f_0 and Δf_a are the signal operating frequency and the frequency interval between adjacent elements, respectively. The element spacing denoted as d which is taken as

$$d = \frac{\lambda_0}{2} = \frac{c}{2f_0}, \tag{2}$$

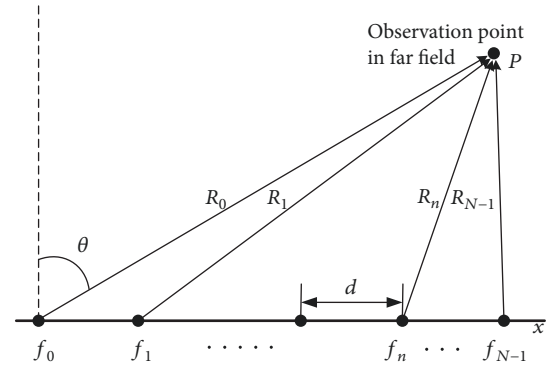

Figure 1: Geometry of FDA.

where c is the velocity of light and λ_0 is the wavelength with respect to the operating frequency f_0. The geometry of FDA is illustrated in Figure 1.

The signal radiated by the nth element can be expressed as

$$x_n(t) = a_n e^{-j2\pi f_n t}, \tag{3}$$

where a_n is the complex weight related to nth transmitted signal. Total electric field observed by a point target $P(\theta, r)$ from far field can be written as

$$x(t, \theta, r) = \sum_{n=0}^{N-1} x_n\left(t - \frac{R_n}{c}\right) = \sum_{n=0}^{N-1} a_n e^{-j2\pi f_n (t-(R_n/c))}, \tag{4}$$

where R_n is the distance between target and nth element; it can be given as $R_n = r - nd\sin\theta$, where θ and $r = R_0$ are the angle and range of the target, respectively.

The phase of nth signal is

$$\phi_n(t) = -2\pi f_n t + \frac{2\pi f_n}{c} R_n. \tag{5}$$

In comparison with the reference and nth signal, the phase difference can be given as

$$\begin{aligned}\Delta\phi_n(t) &= \phi_n(t) - \phi_0(t) \\ &= -2\pi n\left(\Delta f_a t - \frac{r\Delta f_a}{c} + \frac{f_0 d\sin\theta}{c} + n\frac{\Delta f_a d\sin\theta}{c}\right).\end{aligned} \tag{6}$$

The array factor is not just affected by the angle θ, the range r, and frequency increment Δf_a but also plays an important role. Since $nd\sin\theta \ll r$ and $\Delta f_a \ll f_0$, the 4th term of (6) is small and ignorable. So, (6) becomes

$$\Delta\phi_n(t) = -2\pi n\left(\Delta f_a t - \frac{r\Delta f_a}{c} + \frac{f_0 d\sin\theta}{c}\right). \tag{7}$$

After rearranging terms, (4) can be expressed as

$$x(t,\theta,r) = e^{-j2\pi f_0(t-(r/c))} \sum_{n=0}^{N-1} a_n e^{-j2\pi n(\Delta f_a t-(r\Delta f_a/c)+(f_0 d \sin\theta/c))}. \tag{8}$$

The steering vector can be given as

$$\mathbf{a}(t,\theta,r) = \left[1 \quad e^{-j2\pi(\Delta f_a t+(f_0 d \sin\theta/c)-(r\Delta f_a/c))} \quad \cdots \quad e^{-j2\pi(N-1)(\Delta f_a t+(f_0 d \sin\theta/c)-(r\Delta f_a/c))}\right]^{\mathrm{T}}, \tag{9}$$

where $[\cdot]^{\mathrm{T}}$ is the transpose operator. Define the element weighting vector as $\mathbf{w} = [a_0 \quad a_1 \quad \cdots \quad a_{N-1}]^{\mathrm{T}}$. In beamspace design sense, the common factor $\exp(-j2\pi f_0(t-(r/c)))$ can also be ignored in the discussion; (8) simplifies to

$$x(t,\theta,r) = \mathbf{w}^{\mathrm{H}}\mathbf{a}, \tag{10}$$

where $[\cdot]^{\mathrm{H}}$ is the conjugate transpose operator. Consider the case that $a_0 = a_1 = \cdots = a_{N-1} = 1$, the transmit beampattern is given by

$$B(t,\theta,r) = |x(t,\theta,r)| = \left|\frac{\sin[N\pi(\Delta f_a t + f_0 d \sin\theta/c - r\Delta f_a/c)]}{\sin[\pi(\Delta f_a t + f_0 d \sin\theta/c - r\Delta f_a/c)]}\right|, \tag{11}$$

which is the beampattern of FDA radar. Note that if $\Delta f = 0$, the beampattern becomes

$$B(\theta) = \left|\frac{\sin[N\pi(f_0 d \sin\theta/c)]}{\sin[\pi(f_0 d \sin\theta/c)]}\right|, \tag{12}$$

which is only angle dependent just like conventional phased array radar.

3. Mathematical Principle and Design Technique of SFP-FDA Radar

Consider an N element FDA, the frequency transmitted on the nth element in the first pulse of SFP-FDA radar is the same as that of FDA radar, and the frequency of the waveform radiated from each element is incremented by a small amount from pulse to pulse. As shown in Figure 2, the frequency in the mth pulse of the nth element can be given as

$$f_{nm} = f_0 + n\Delta f_a + m\Delta f_t \quad m = 0, 1, \ldots, M-1, \tag{13}$$

where Δf_t is the frequency interval between adjacent pulses, and M is the number of the transmit pulses.

Adopting the signal of the nth element, the electric field observed by $P(\theta, r)$ can be taken as

$$x_n(t,r) = \sum_{m=0}^{M-1} \frac{a_{nm}}{R_n} \exp\left\{-j2\pi\left[f_{nm}\left(t - mT_p - \frac{R_n}{c}\right)\right]\right\}, \tag{14}$$

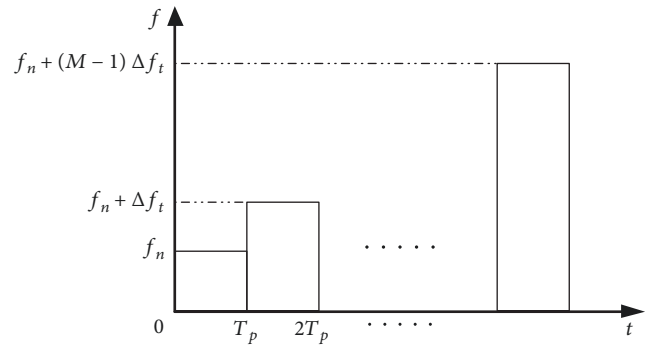

Figure 2: Frequency increment versus time in the nth element.

where T_p is the pulse width, and a_{nm} is the complex weight of mth pulse associated with nth transmitted signal. Substituting $R_n = r - nd \sin\theta$ and (13) into (14) yields

$$x_n(t,r) = \sum_{m=0}^{M-1} \frac{a_{nm}}{r - nd\sin\theta} \exp\left\{-j2\pi\left[(f_0 + n\Delta f_a + m\Delta f_t) \cdot \left(t - mT_p - \frac{r - nd\sin\theta}{c}\right)\right]\right\}. \tag{15}$$

Assuming $\Delta f_a \ll 1/T_p$ and $\Delta f_t \ll 1/T_p$, then let T_p satisfied with $f_0 T_p$ = integer. Due to the fact that $\exp\{jx\}$ is a periodic function with a period of 2π, so $\exp\{-j2\pi[(f_0 + n\Delta f_a + m\Delta f_t)(mT_p)]\} \approx \exp\{-j2\pi \times 0\}$ can be approximately obtained. Furthermore, in the sense of amplitude, we can utilize $R_n \approx r$ as approximation. Then, (15) can be equivalently reformulated as

$$\begin{aligned} x_n(t,\theta,r) &= \frac{1}{r}\sum_{m=0}^{M-1} a_{nm} \exp\left\{-j2\pi\left[(f_0 + n\Delta f_a + m\Delta f_t) \cdot \left(t - \frac{r - nd\sin\theta}{c}\right)\right]\right\} \\ &= \frac{\exp(j\phi_0)}{r}\sum_{m=0}^{M-1} a_{nm} \exp\left\{-j2\pi\left(n\Delta f_a t + m\Delta f_t t - n\Delta f_a \frac{r}{c} - m\Delta f_t \frac{r}{c} + f_0 \frac{nd\sin\theta}{c} + \frac{n^2\Delta f_a d\sin\theta}{c} + \frac{mn\Delta f_t d\sin\theta}{c}\right)\right\}, \end{aligned} \tag{16}$$

where $\phi_0 = -2\pi f_0(t - r/c)$. Similarly, $nd\sin\theta \ll r$ and $\Delta f_a \ll f_0$; also, we assumed that $\Delta f_t \ll f_0$, and then the terms $n^2\Delta f_a d\sin\theta/c$ and $mn\Delta f_t d\sin\theta/c$ are small and can be ignored. The common factor $\exp(j\phi_0)/r$ can also be ignored in the sense of beamspace design. And the corresponding transmit beampattern can be written as

$$A(t,\theta,r)=\left|\sum_{n=0}^{N-1}x_n(t,\theta,r)\right| =\left|\sum_{n=0}^{N-1}\sum_{m=0}^{M-1}a_{nm}\exp\left\{-j2\pi\left(n\Delta f_a t - n\Delta f_a\frac{r}{c}+f_0\frac{nd\sin\theta}{c}\right)\right\}\exp\cdot\left\{-j2\pi\left(m\Delta f_t t - m\Delta f_t\frac{r}{c}\right)\right\}\right|. \tag{17}$$

Provided that the weights of signals' pulses with the same order number in each element are equal. And $\mathbf{w}_t$ and $\mathbf{w}_a$ are defined as the signal weighting vector and the element weighting vector, respectively. Taking $\otimes$ as the Kronecker product operator, (17) can be rewritten as

$$\begin{aligned}A(t,\theta,r)&=\left|\mathbf{w}_a^{\mathrm{H}}\boldsymbol{\alpha}_a(t,\theta,r)\mathbf{w}_t^{\mathrm{H}}\boldsymbol{\alpha}_t(t,r)\right|\\&=\left|\mathbf{w}^{\mathrm{H}}[\boldsymbol{\alpha}_a(t,\theta,r)\otimes\boldsymbol{\alpha}_t(t,r)]\right|\\&=\left|\mathbf{w}^{\mathrm{H}}\boldsymbol{\alpha}(t,\theta,r)\right|,\end{aligned} \tag{18}$$

where $\boldsymbol{\alpha}(t,\theta,r)=\boldsymbol{\alpha}_a(t,\theta,r)\otimes\boldsymbol{\alpha}_t(t,r)$ and

$$\begin{aligned}\boldsymbol{\alpha}_a(t,\theta,r)&=\left[1\quad\cdots\quad\exp\left\{-j2\pi(N-1)\cdot\left(\Delta f_a t-\Delta f_a\frac{r}{c}+f_0\frac{d\sin\theta}{c}\right)\right\}\right]^{\mathrm{T}},\\\boldsymbol{\alpha}_t(t,r)&=\left[1\quad\cdots\quad\exp\left\{-j2\pi(M-1)\cdot\left(\Delta f_t t-\Delta f_t\frac{r}{c}\right)\right\}\right]^{\mathrm{T}},\\\mathbf{w}=\mathbf{w}_a\otimes\mathbf{w}_t&=\left[w_{00}\quad\cdots\quad w_{0,M-1}\quad\cdots\quad w_{nm}\cdots w_{N-1,M-1}\right]^{\mathrm{T}}.\end{aligned} \tag{19}$$

This implies that by optimizing $\mathbf{w}_a$ and $\mathbf{w}_t$, the transmit beampattern can be schemed out.

Consider the case that $a_{00}=a_{01}=\cdots=a_{N-1,M-1}=1$, the beampattern (17) is then shown to be

$$\begin{aligned}A(t,\theta,r)&=\left|\sum_{n=0}^{N-1}\exp\left\{-j2\pi\left(n\Delta f_a t-n\Delta f_a\frac{r}{c}+f_0\frac{nd\sin\theta}{c}\right)\right\}\cdot\sum_{m=0}^{M-1}\exp\left\{-j2\pi\left(m\Delta f_t t-m\Delta f_t\frac{r}{c}\right)\right\}\right|\\&=\left|AF_1(t,\theta,r)\cdot AF_2(t,r)\right|,\end{aligned} \tag{20}$$

where

$$\begin{aligned}AF_1(t,\theta,r)&=\frac{\sin\left[N\pi(\Delta f_a t-\Delta f_a(r/c)+f_0(d\sin\theta/c))\right]}{\sin\left[\pi(\Delta f_a t-\Delta f_a(r/c)+f_0(d\sin\theta/c))\right]},\\AF_2(t,r)&=\frac{\sin\left[M\pi(\Delta f_t t-\Delta f_t(r/c))\right]}{\sin\left[\pi(\Delta f_t t-\Delta f_t(r/c))\right]}.\end{aligned} \tag{21}$$

Note that when $\Delta f_t=0$, we can get $A(t,\theta,r)=|AF_1(t,\theta,r)|$, that is, the expression of the conventional FDA. And if $\Delta f_a=\Delta f_t=0$, (20) is equivalent to (12). Therefore, the phased array radar and FDA radar can be regarded as two special forms of SFP-FDA. Assume that $\theta_0=0$, $r_0=0$, and $t_0=1/(\Delta f_a,\Delta f_t)$, where $(\Delta f_a,\Delta f_t)$ is the greatest common divisor (GCD) of Δf_a and Δf_t. For a given range and time, namely, $r=r_0$ and $t=t_0$, we then have $AF_2(t,r)=1$; (20) will be equivalent to conventional FDA. Under these circumstances, both the FDA radar and the SFP-FDA radar have the same expression; hence, they possess the same angle resolution. According to [32, 33], the function $G(x)$ can be defined as

$$G(x)=\left|\frac{\sin\left[N\pi x\right]}{\sin\left[\pi x\right]}\right|. \tag{22}$$

Its 3 dB resolution can be calculated as

$$\left\{\left|\frac{\sin\left[N\pi x_{0.5}\right]}{\sin\left[\pi x_{0.5}\right]}\right|^2=0.5,\quad N\pi x_{0.5}=1.392,\ x_{mb}=2x_{0.5}.\right. \tag{23}$$

To calculate the range resolution, (11) can be simplified to

$$B(t_0,\theta_0,r)=\left|\frac{\sin\left[N\pi(r\Delta f_a/c)\right]}{\sin\left[\pi(r\Delta f_a/c)\right]}\right|. \tag{24}$$

Then, the 3 dB range resolution of FDA can be given as

$$r_{\mathrm{FDA}}=\frac{2.784c}{\pi N\Delta f_a}. \tag{25}$$

Similarly, (20) can be simplified to

$$A(t_0,\theta_0,r)=\left|\frac{\sin\left[N\pi(\Delta f_a(r/c))\right]}{\sin\left[\pi(\Delta f_a(r/c))\right]}\cdot\frac{\sin\left[M\pi(\Delta f_t(r/c))\right]}{\sin\left[\pi(\Delta f_t(r/c))\right]}\right|. \tag{26}$$

Assuming that $M=\delta_1 N$ and $\Delta f_t=\delta_2\Delta f_a$, (26) can be equivalently reformulated as

$$A(t_0,\theta_0,r)=\left|\frac{\sin\left[N\pi x\right]}{\sin\left[\pi x\right]}\cdot\frac{\sin\left[\delta_1 N\pi(\delta_2 x)\right]}{\sin\left[\pi(\delta_2 x)\right]}\right|, \tag{27}$$

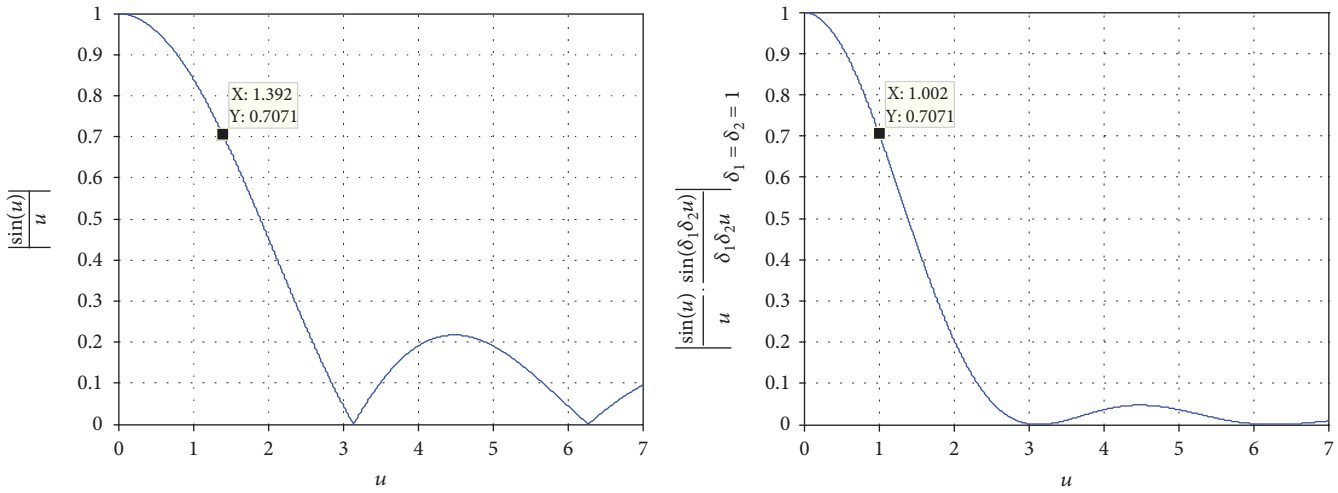

Figure 3: Function value diagram: (a) $|\sin(u)/u|$ and (b) $|(\sin(u)/u)(\sin(\delta_1\delta_2 u)/\delta_1\delta_2 u)|_{\delta_1=\delta_2=1}$.

where $x = \Delta f_a r/c$. Taking $\delta_1 = 1$ and $\delta_2 = 1$ as an example, assuming $u = N\pi x$, we can plot Figure 3.

Then, the 3 dB range resolution of SFP-FDA can be given as

$$r_{\text{SFP-FDA}} = \frac{2.004c}{\pi N \Delta f_a}. \tag{28}$$

The range resolution depends on M, N, Δf_t, and Δf_a. The second factor of (26) is satisfied with

$$\left|\frac{\sin\left[M\pi(\Delta f_t(r/c))\right]}{M\sin\left[\pi(\Delta f_t(r/c))\right]}\right| \le 1. \tag{29}$$

Then, we will have $u_{\text{SFP-FDA}} < u_{\text{FDA}}$, where $u_{\text{SFP-FDA}}$ and u_{FDA} are the values of u when $Y = 0.7071$ (Figure 3) in SFP-FDA and FDA, respectively; we can also obtain identical conclusion by comparing (25) and (28). Therefore, SFP-FDA outperforms FDA in range resolution.

4. Target Localization in Angle-Range Dimensions

Consider the SFP-FDA with N elements and M pulses, the transmitted signal can be expressed as

$$\mathbf{x}(t,\theta,r) = \sum_{n=0}^{N-1}\left[\mathbf{w}_n^{\text{H}}\boldsymbol{\alpha}_n(\theta,r)\right]s_n(t). \tag{30}$$

The reflected signal is formed as a result of delay and attenuation of the transmitted signal.

$$\mathbf{x}_r(t,\theta,r) = \sigma(\theta,r)\sum_{n=0}^{N-1}\left[\mathbf{w}_n^{\text{H}}\boldsymbol{\alpha}_n(\theta,r)e^{-j\Delta_n(\theta,r)}\right]s(t), \tag{31}$$

where $\sigma(\theta,r)$ is the complex reflection amplitudes from the target in (θ,r); $\mathbf{w}_n$ and $\boldsymbol{\alpha}_n$ are the signal weighting vector and transmit steering vector of nth array element, respectively. $\Delta_n(\theta,r)$ is the propagation delay in nth array element. $s(t)$ is the baseband waveform. We assumed

$$\mathbf{g}_r(t,\theta,r) = \sum_{n=0}^{N-1}\left[\mathbf{w}_n^{\text{H}}\boldsymbol{\alpha}_n(\theta,r)e^{-j\Delta_n(\theta,r)}\right]. \tag{32}$$

The demodulated baseband received signal can be written as

$$\mathbf{y} = \sigma(\theta,r)\mathbf{g}_r(t,\theta,r)\otimes\mathbf{v}(t,\theta,r) + \mathbf{n}, \tag{33}$$

where $\mathbf{v}(t,\theta,r)$ and $\mathbf{n}$ are the received steering vector and normalized Gaussian noise vector, respectively. The steering vector of transmit-receive can be written as

$$\mathbf{u}(t,\theta,r) = \mathbf{g}_r(t,\theta,r)\otimes\mathbf{v}(t,\theta,r). \tag{34}$$

The traditional nonadaptive receive beamforming is used, i.e., the weighting vector $\mathbf{w}_R = \mathbf{u}(t_0,\theta_s,r_s)$, where θ_s and r_s denote the far field target's angle and range, respectively. The received beampattern can be given as [34]

$$\mathbf{B}(\theta,r) = \frac{\left|\mathbf{w}_r^{\text{H}}\mathbf{u}(t_0,\theta,r)\right|^2}{\left|\mathbf{w}_r^{\text{H}}\mathbf{u}(t_0,\theta_s,r_s)\right|^2} = \frac{\left|\mathbf{u}^{\text{H}}(t_0,\theta_s,r_s)\mathbf{u}(t_0,\theta,r)\right|^2}{\left\|\mathbf{u}(t_0,\theta_s,r_s)\right\|^4}. \tag{35}$$

Note that if there are multiple targets such as three targets with the coordinates being (θ_{s1},r_{s1}), (θ_{s2},r_{s2}), and (θ_{s3},r_{s3}), the weighting vector will change to

$$\mathbf{w}_R = \mathbf{u}(t_0,\theta_{s1},r_{s1}) + \mathbf{u}(t_0,\theta_{s2},r_{s2}) + \mathbf{u}(t_0,\theta_{s3},r_{s3}). \tag{36}$$

According to analysis of Section 3 and Section 4, the data model of received signal can be written as

$$\mathbf{y}_l = \sigma_0 \mathbf{u}(\theta_s, r_s) + \mathbf{n}, \tag{37}$$

where $\mathbf{u}(\theta_s, r_s) = \boldsymbol{\alpha}(t_0, \theta_s, r_s)$, and σ_0 is the complex amplitudes.

For a nonadaptive beamformer, the weighting vector $\mathbf{w}_R = \mathbf{u}(\theta_s, r_s)$ and the angle and range of the target can be estimated as

$$\begin{cases} \widehat{\theta}_s = \arg\left\{ \max\limits_{\theta_s} \left| \mathbf{w}_R^{\mathrm{H}} \mathbf{y}_l \right|^2 \right\} \\ \widehat{r}_s = \arg\left\{ \max\limits_{r_s} \left| \mathbf{w}_R^{\mathrm{H}} \mathbf{y}_l \right|^2 \right\}. \end{cases} \tag{38}$$

Owing to the decoupling transmit beampattern of the SFP-FDA radar, the angle and range of the target can be simultaneously estimated by utilizing only one step.

5. Performance Analysis

An analytical comparison of the performance of the proposed system and the double-pulse FDA radar in terms of CRLB is conducted; we rewrite (37) as

$$\mathbf{y}_p = \sqrt{\mathrm{SNR}} \cdot \mathbf{u}_r(\theta_s, r_s) + \mathbf{n}, \tag{39}$$

where $\mathbf{u}_r(\theta_s, r_s)$ and SNR are the equivalent receiver steering vector and the signal to noise ratio, respectively. And the mean and variance of $\mathbf{n}$ are zero and $\mathbf{I}$. $\mathbf{u}_r(\theta_s, r_s) = \mathbf{u}_{\text{SFP-FDA}}(\theta_s, r_s)$ and $\mathbf{u}_r(\theta_s, r_s) = \mathbf{u}_{\text{FDA}}(\theta_s, r_s)$ are defined under the circumstances of SFP-FDA radar and the double-pulse FDA radar, respectively. A closed-form CRLB can be deducted approximately by arranging the steering vectors.

$$\begin{aligned} \mathbf{u}_{\text{SFP-FDA}}(\theta_s, r_s) &= \left[\mathbf{u}(\theta_s, r_s)|_{\omega_0}, \dots, \mathbf{u}(\theta_s, r_s)|_{\omega_{M-1}} \right]^{\mathrm{T}} \\ &\approx \left[e^{-j\omega_0(0)}, \dots, e^{-j\omega_0(N-1)}, \dots, \right. \\ &\quad \left. e^{-j\omega_{M-1}(0)}, \dots, e^{-j\omega_{M-1}(N-1)} \right]^{\mathrm{T}}. \end{aligned} \tag{40}$$

On the other hand,

$$\begin{aligned} \mathbf{u}_{\text{FDA}}(\theta_s, r_s) &= \left[\mathbf{u}(\theta_s, r_s)|_{\omega_{00}}, \mathbf{u}(\theta_s, r_s)|_{\omega_0} \right]^{\mathrm{T}} \\ &\approx \left[e^{-j\omega_{00}(0)}, \dots, e^{-j\omega_{00}(N-1)}, \right. \\ &\quad \left. e^{-j\omega_0(0)}, \dots, e^{-j\omega_0(N-1)} \right]^{\mathrm{T}}, \end{aligned} \tag{41}$$

where

$$\begin{aligned} \omega_{00}(n) &= n \frac{2\pi f_0 d \sin\theta_s}{c}, \\ \omega_0(n) &= n \frac{2\pi (f_0 + \Delta f_a) d \sin\theta_s}{c} - n \frac{2\pi \Delta f_a r_s}{c}, \\ \omega_1(n) &= n \frac{2\pi (f_0 + \Delta f_a + \Delta f_t) d \sin\theta_s}{c} \\ &\quad - n \frac{2\pi \Delta f_a r_s}{c} - \frac{2\pi \Delta f_t r_s}{c}, \\ &\vdots \\ \omega_{M-1}(n) &= n \frac{2\pi [f_0 + \Delta f_a + (M-1)\Delta f_t] d \sin\theta_s}{c} \\ &\quad - n \frac{2\pi \Delta f_a r_s}{c} - (M-1) \frac{2\pi \Delta f_t r_s}{c}. \end{aligned} \tag{42}$$

The mean $\boldsymbol{\mu}$ and covariance $\boldsymbol{\Gamma}$ of $\mathbf{y}_p$ can be respectively expressed as

$$\begin{aligned} \boldsymbol{\mu} &= \mathbf{u}_r(\theta_s, r_s) \sqrt{\mathrm{SNR}}, \\ \boldsymbol{\Gamma} &= \mathbf{I}. \end{aligned} \tag{43}$$

The Fisher information matrix (FIM) can be obtained by [35].

$$\mathbf{J} = 2\ \mathrm{Re}\left[\frac{d\boldsymbol{\mu}^*}{d\boldsymbol{\eta}} \boldsymbol{\Gamma}^{-1} \frac{d\boldsymbol{\mu}}{d\boldsymbol{\eta}^{\mathrm{T}}} \right], \tag{44}$$

where

$$\boldsymbol{\eta} = [\theta_s, r_s]^{\mathrm{T}}. \tag{45}$$

Then, the FIM of SFP-FDA can be written as

$$\begin{aligned} &\mathbf{J}_{\text{SFP-FDA}} \\ &\quad = 2 \cdot \mathrm{SNR} \\ &\quad \cdot \begin{bmatrix} \sum\limits_{m=0}^{M-1} \sum\limits_{n=0}^{N-1} \left[k_m^2(n) \right] & \sum\limits_{m=0}^{M-1} \sum\limits_{n=0}^{N-1} \left[k_m(n) \cdot \xi_m(n) \right] \\ \sum\limits_{m=0}^{M-1} \sum\limits_{n=0}^{N-1} \left[k_m(n) \cdot \xi_m(n) \right] & \sum\limits_{m=0}^{M-1} \sum\limits_{n=0}^{N-1} \left[\xi_m^2(n) \right] \end{bmatrix}, \end{aligned} \tag{46}$$

where

$$k_0(n) = n \frac{2\pi (f_0 + \Delta f_a) d \cos\theta_s}{c},$$

$$k_1(n) = n \frac{2\pi (f_0 + \Delta f_a + \Delta f_t) d \cos\theta_s}{c},$$

$$\vdots$$

$$k_{M-1}(n) = n\frac{2\pi[f_0 + \Delta f_a + (M-1)\Delta f_t]d\cos\theta_s}{c},$$
$$\xi_0(n) = -n\frac{2\pi\Delta f_a r_s}{c},$$
$$\xi_1(n) = -n\frac{2\pi\Delta f_a r_s}{c} - \frac{2\pi\Delta f_t r_s}{c},$$
$$\vdots$$
$$\xi_{M-1}(n) = -n\frac{2\pi\Delta f_a r_s}{c} - (M-1)\frac{2\pi\Delta f_t r_s}{c}. \quad (47)$$

By calculating the inverse matrix of FIM, the CRLB for the target's estimation in angle and range domains can be obtained as

$$\mathrm{CRLB}_{\theta_s} = \left[\mathbf{J}^{-1}_{\text{SFP-FDA}}\right]_{1,1},$$
$$\mathrm{CRLB}_{r_s} = \left[\mathbf{J}^{-1}_{\text{SFP-FDA}}\right]_{2,2}, \quad (48)$$

where $[\cdot]_{i,j}$ represents the element in the ith row and jth column of the matrix. The performance comparison of the two radars is presented in simulations.

6. Numerical Results

Consider a linear array of 16 elements with interelement spacing $d = 0.5\lambda_0$. The carrier frequency is $f_0 = 6$ GHz, whereas the frequency interval between adjacent elements and pulses is $\Delta f_a = \Delta f_t = 3$ kHz. The number of pulses is $M = 16$, and pulse width is $T_p = 2\,\mu$s. The additive noise is modeled as complex Gaussian zero-mean spatially and temporally white random sequences with identical variance at each antenna element.

6.1. One Target. In the first part of this section, suppose that the target of interest is located in the angle $\theta_{s1} = 0^\circ$ and the slant range $r_{s1} = 50$ km. The comparative target responses of the FDA radar and SFP-FDA are shown in Figure 4. In the FDA radar, owing to the angle-range coupling, the target cannot be localized effectively in both domains. Using the double-pulse FDA approach proposed in [31], the target angle can be estimated to be $\widehat{\theta}_s = 0^\circ$ by using the first pulse which can be seen as phased array, and then the target range can be estimated to be $\widehat{r}_s = 50$ km by taking advantage of the second pulse with FDA, as shown in Figure 5. Similarly, using the method mentioned in Section 4, as shown in Figure 6, we can localize the target in angle-range dimensions as $(0^\circ, 50$ km). Note that the pulse number M, the element number N, and the frequency increments Δf_t and Δf_a all affect the range resolution.

While compared with the double-pulse FDA radar, our proposed scheme has lower sidelobe and more concentrated energy in the mainlobe area. Besides, different from FDA radar, SFP-FDA radar has a range-angle decoupling beampattern.

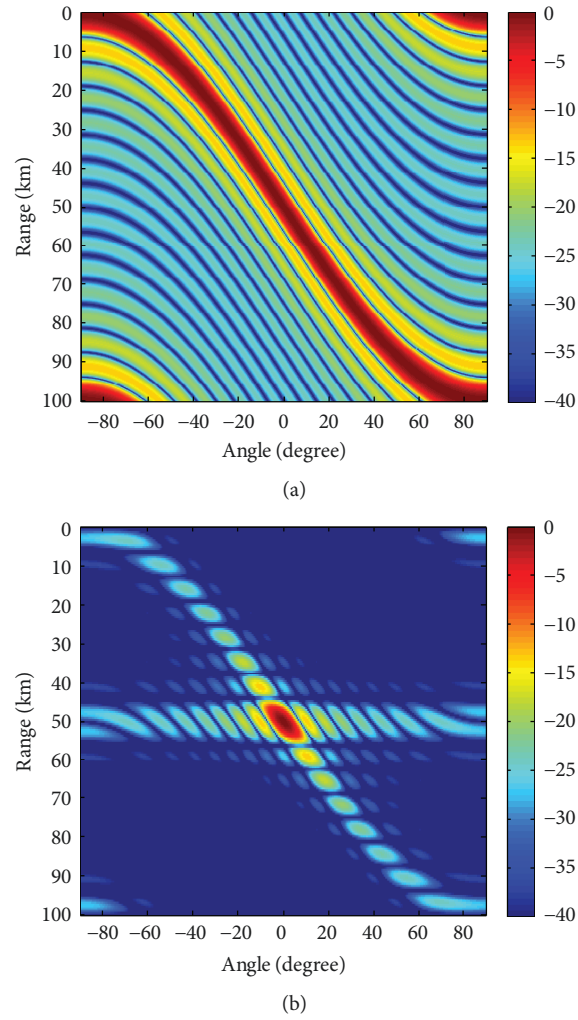

Figure 4: Comparative target response: (a) FDA radar and (b) SFP-FDA radar.

SFP-FDA radar can estimate the coordinates of target by only one step, whereas the double-pulse FDA radar demands two steps.

By comparing Figure 5 with Figure 6, it can be observed that, despite the equal angle response of both the radars, the SFP-FDA outperforms the FDA in the range profile, i.e., the former has a narrower mainlobe and much lower sidelobe.

Then, we plotted Figure 7, which compared the 3 dB resolution performance of FDA and SFP-FDA. Clearly, the advantage of SFP-FDA in range dimension can be observed, which is consistent with the theoretical analysis in Section 3.

6.2. Two Targets with Different Angle and Different Range. Assuming that the two targets are located in coordinates $(\theta_{s1}, r_{s1}) = (0^\circ, 50\,\text{km})$ and $(\theta_{s2}, r_{s2}) = (30^\circ, 60\,\text{km})$. Figure 8 gives the target response of FDA radar and SFP-FDA radar. Since the two targets have different angle, it can be noticed that due to the angle-range coupling, it is very difficult

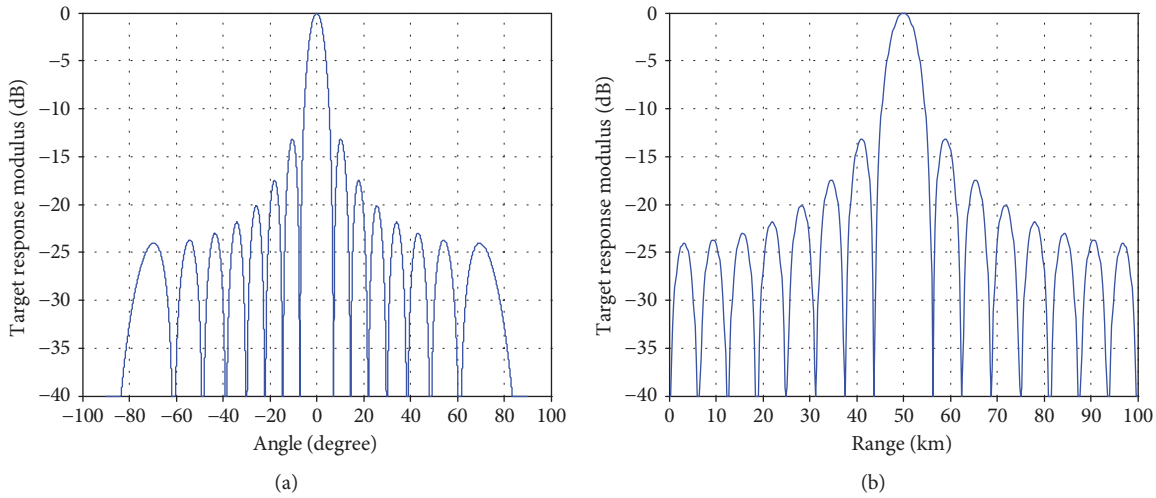

Figure 5: Target response by double-pulse FDA radar: (a) the first step and (b) the second step.

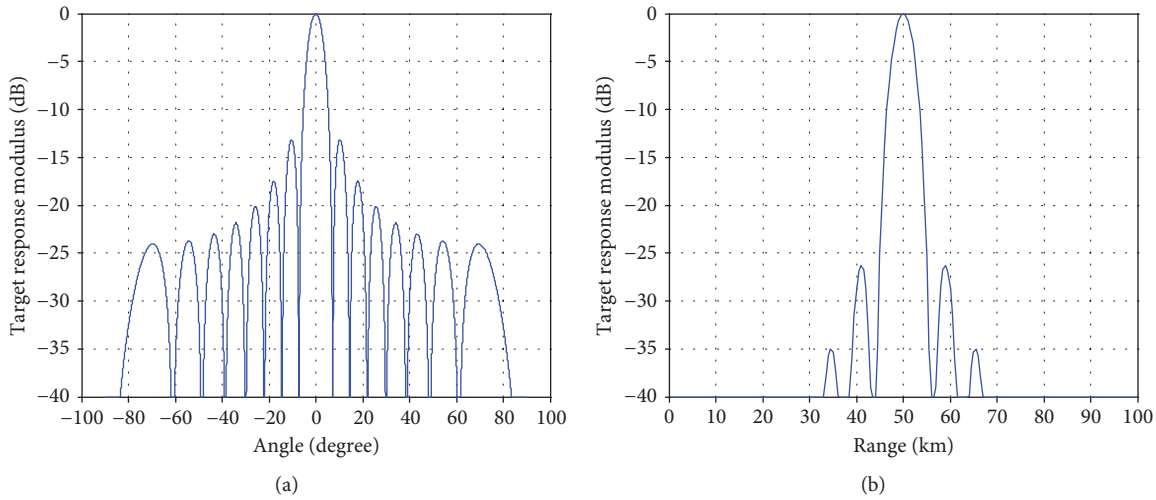

Figure 6: Target response by SFP-FDA radar: (a) the angle profile and (b) the range profile.

to separate the peaks in both angle and range domains from the FDA beamformer output.

By utilizing the first step of the double-pulse FDA radar, the angle of the targets can be received, namely, 0° and 30°. But when the second step is carried out, there are two peaks in each angle, as shown in Figure 9; thus, four targets have been obtained, and we cannot distinguish which ones are the real ones. The four targets can then be localized in angle-range dimensions as (0°, 50 km), (0°, 35 km), (30°, 60 km), and (30°, 75 km). Furthermore, by this means, we cannot accurately identify whether there are 2 targets, 3 targets, or even 4 targets.

Figures 10 and 11 give the target response of SFP-FDA radar, the two targets can be directly identified both in the angle and range dimensions, and then they can be localized in (0°, 50 km) and (30°, 60 km).

It is evident that the two targets can be easily distinguished by the proposed scheme, which demonstrates the effectiveness of the SFP-FDA radar in resolving multiple targets. This simulation example shows that the SFP-FDA radar achieves better performance than the double-pulse FDA radar.

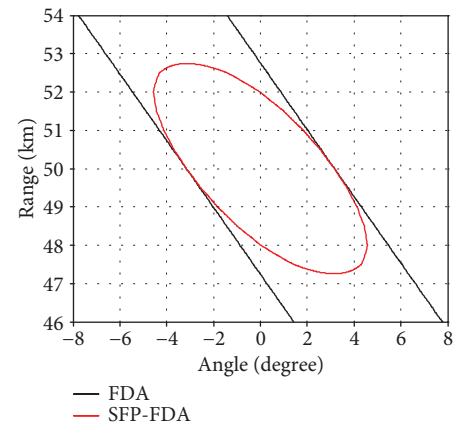

Figure 7: Comparative 3 dB resolution of FDA and SFP-FDA.

6.3. Estimation Performance. In this subsection, as compared to the double-pulse FDA radar, we simulated the performance of the proposed angle-range localization approach in

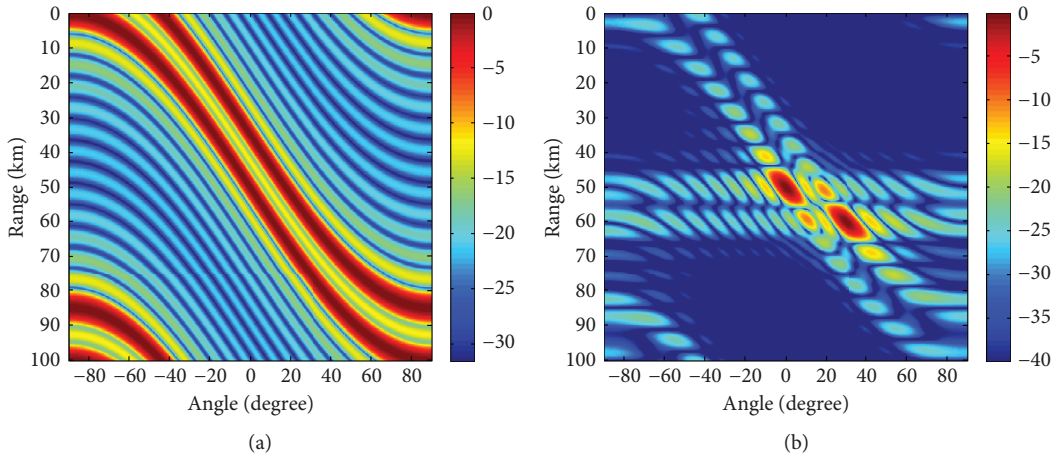

Figure 8: Comparative target response of two targets: (a) FDA radar and (b) SFP-FDA radar.

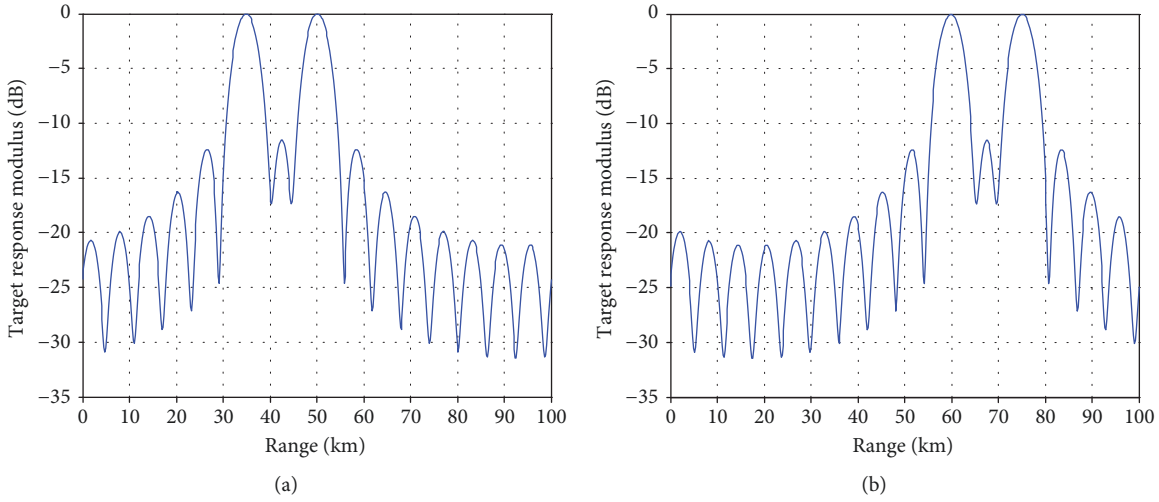

Figure 9: Range response of double-pulse FDA in the second processing step: (a) $\theta_{s1} = 0^\circ$ and (b) $\theta_{s2} = 30^\circ$.

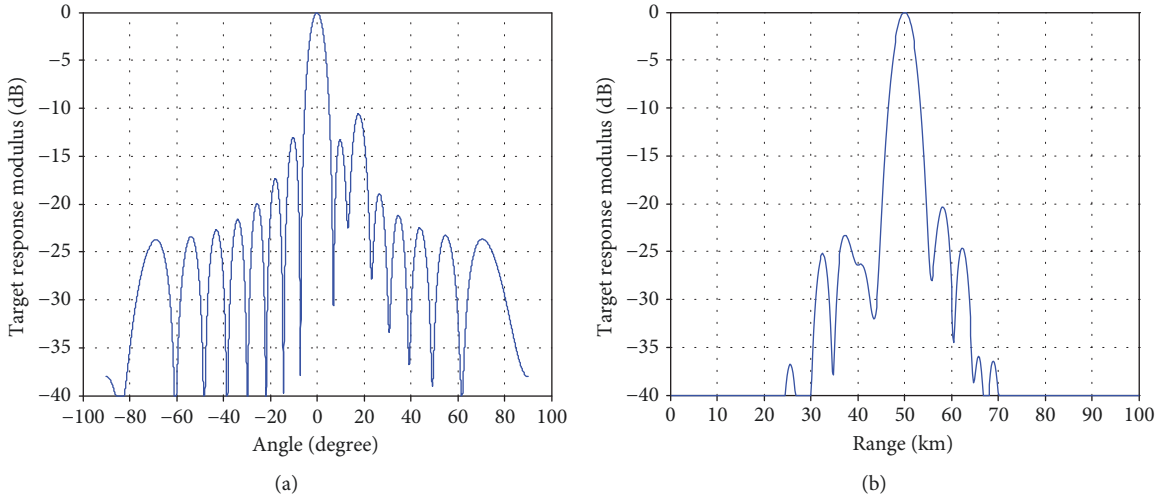

Figure 10: The first target response: (a) the angle profile and (b) the range profile.

terms of CRLB. Figure 12 shows the comparative performance of localization as a function of the SNR between the proposed scheme and the double-pulse FDA radar.

Figures 12(a) and 12(b) show the CRLB in the angle and range domain, respectively. It can be seen that the SFP-FDA radar can achieve a better estimation performance in both

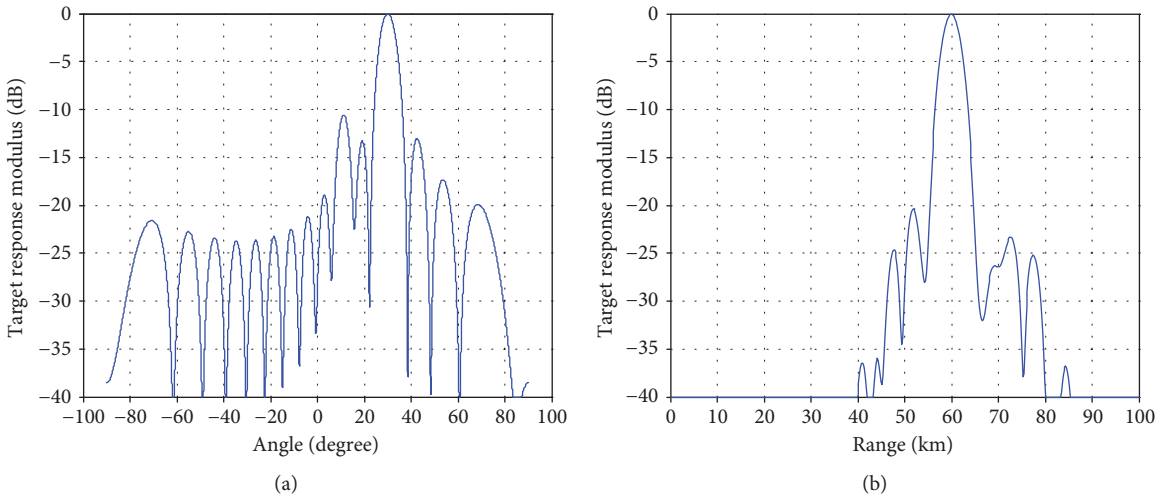

Figure 11: The second target response: (a) the angle profile and (b) the range profile.

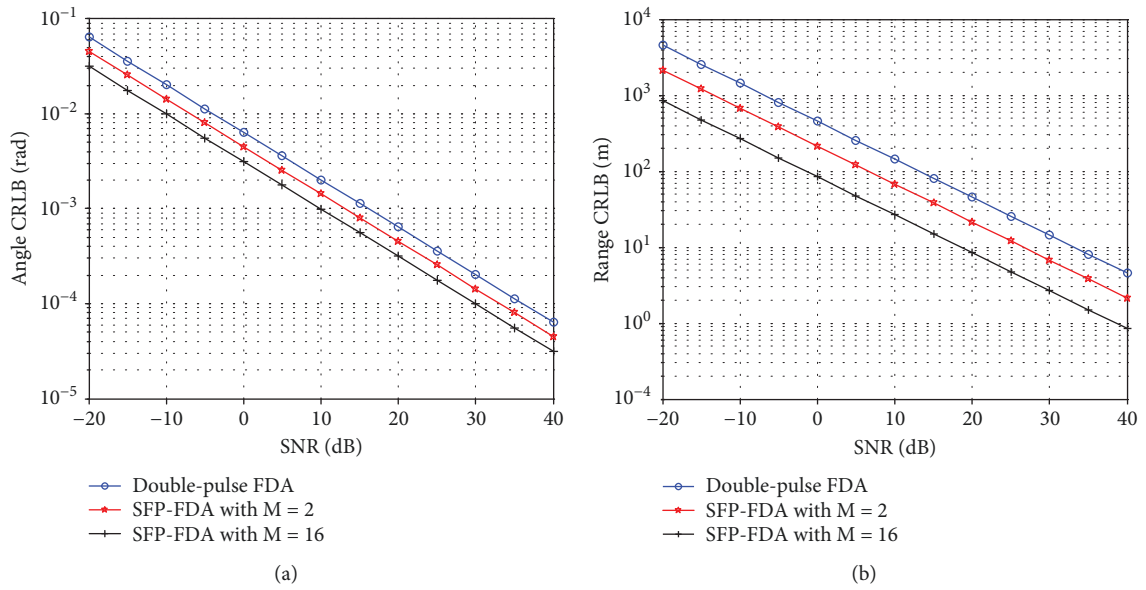

Figure 12: Comparative performance of range-angle localization: (a) the angle domain and (b) the range domain.

angle and range dimension, even when the number of its pulses is the same as that of the double-pulse FDA radar, that is, when $M = 2$. Moreover, it is evident that the performance of both in the angle and range domains is improved as the SNR and the number of pulses increase. As shown in Figure 12, the SFP-FDA with $M = 16$ performs better than the SFP-FDA with $M = 2$. It is clear that the SFP-FDA radar achieves better estimation performance at the cost of much higher computation complexity.

7. Conclusion

Since the beampattern produced by conventional FDA is angle-range coupling, a novel scheme called stepped frequency pulse FDA radar is proposed in this paper, which can decouple the angle and range responses in the transmit beamforming. Only one step procedure is needed to localize the targets in angles and ranges simultaneously, and the range resolution of targets outperforms that of double-pulse FDA radar. The proposed system has a stronger ability in identifying the multiple targets with different angles and different ranges. It has also been shown that the proposed radar achieves a better CRLB performance than the double-pulse FDA radar, though at the expense of a certain amount of computational complexity. Certainly, further investigations will consider the Doppler of targets. With new application potentials, combining with netted radar networks and MIMO radar technology can effectively improve the radar performance, and it can also be investigated in a future work.

Data Availability

The data used to support the findings of this study are available from the corresponding author upon request.

Conflicts of Interest

The authors declare that there are no conflicts of interest regarding the publication of this paper.

Acknowledgments

This work was supported by the National Natural Science Foundation of China (grant no. 61601502).

References

[1] F. Bandiera, M. Mancino, and G. Ricci, "Localization strategies for multiple point-like radar targets," *IEEE Transactions on Signal Processing*, vol. 60, no. 12, pp. 6708–6712, 2012.

[2] J. Li, G. Liu, N. Jiang, and P. Stoica, "Moving target feature extraction for airborne high-range resolution phased-array radar," *IEEE Transactions on Signal Processing*, vol. 49, no. 2, pp. 277–289, 2001.

[3] S. Haykin, J. Litva, and T. J. Shepherd, *Radar Array Processing*, Springer, New York, NY, USA, 1993.

[4] P. Rocca, R. L. Haupt, and A. Massa, "Interference suppression in uniform linear arrays through a dynamic thinning strategy," *IEEE Transactions on Antennas and Propagation*, vol. 59, no. 12, pp. 4525–4533, 2011.

[5] T. F. Chun, A. Zamora, Bao Jun Lei, R. T. Iwami, and W. A. Shiroma, "An interleaved, interelement phase-detecting/phase-shifting retrodirective antenna array for interference reduction," *IEEE Antennas and Wireless Propagation Letters*, vol. 10, pp. 919–922, 2011.

[6] Y.-Y. Bai, S. Xiao, M.-C. Tang, Z.-F. Ding, and B.-Z. Wang, "Wide-angle scanning phased array with pattern reconfigurable elements," *IEEE Transactions on Antennas and Propagation*, vol. 59, no. 11, pp. 4071–4076, 2011.

[7] P. Antonik, M. C. Wicks, H. D. Griffiths, and C. J. Baker, "Frequency diverse array radars," in *2006 IEEE Conference on Radar*, pp. 215–217, Verona, NY, USA, April 2006.

[8] P. Antonik, M. C. Wicks, H. D. Griffiths, and C. J. Baker, "Multi-mission multi-mode waveform diversity," in *2006 IEEE Conference on Radar*, pp. 580–582, Verona, NY, USA, April 2006.

[9] P. Antonik and M. C. Wicks, "Method and apparatus for simultaneous synthetic aperture and moving target indication," U. S. Patent 8803732, 2008.

[10] P. Antonik, *An Investigation of a Frequency Diverse Array*, Ph.D., University College London, London, U. K., 2009.

[11] J. Xu, G. Liao, S. Zhu, and H. C. So, "Deceptive jamming suppression with frequency diverse MIMO radar," *Signal Processing*, vol. 113, pp. 9–17, 2015.

[12] P. Baizert, T. B. Hale, M. A. Temple, and M. C. Wicks, "Forward-looking radar GMTI benefits using a linear frequency diverse array," *Electronics Letters*, vol. 42, no. 22, pp. 1311-1312, 2006.

[13] J. Xu, G. Liao, S. Zhu, L. Huang, and H. C. So, "Joint range and angle estimation using MIMO radar with frequency diverse array," *IEEE Transactions on Signal Processing*, vol. 63, no. 13, pp. 3396–3410, 2015.

[14] S. Qin, Y. D. Zhang, M. G. Amin, and F. Gini, "Frequency diverse coprime arrays with coprime frequency offsets for multi-target localization," *IEEE Journal of Selected Topics in Signal Processing*, vol. 11, no. 2, pp. 321–335, 2017.

[15] W. Q. Wang, "Overview of frequency diverse array in radar and navigation applications," *IET Radar, Sonar & Navigation*, vol. 10, no. 6, pp. 1001–1012, 2016.

[16] W. Q. Wang, H. C. So, and A. Farina, "An overview on time/frequency modulated array processing," *IEEE Journal of Selected Topics in Signal Processing*, vol. 11, no. 2, pp. 228–246, 2017.

[17] H. C. So, M. G. Amin, S. Blunt, F. Gini, and W. Q. Wang, "Introduction to the special issue on time/frequency modulated array signal processing," *IEEE Journal of Selected Topics in Signal Processing*, vol. 11, no. 2, pp. 225–227, 2017.

[18] A. Basit, W. Khan, S. Khan, and I. M. Qureshi, "Development of frequency diverse array radar technology: a review," *IET Radar, Sonar & Navigation*, vol. 12, no. 2, pp. 165–175, 2018.

[19] W. Q. Wang, H. Shao, and J. Cai, "Range-angle-dependent beamforming by frequency diverse array antenna," *International Journal of Antennas and Propagation*, vol. 2012, Article ID 760489, 10 pages, 2012.

[20] C. Cetintepe and S. Demir, "Multipath characteristics of frequency diverse arrays over a ground plane," *IEEE Transactions on Antennas and Propagation*, vol. 62, no. 7, pp. 3567–3574, 2014.

[21] Y. Wang, W. Q. Wang, and H. Shao, "Frequency diverse array radar Cramér-Rao lower bounds for estimating direction, range, and velocity," *International Journal of Antennas and Propagation*, vol. 2014, Article ID 830869, 15 pages, 2014.

[22] B. Chen, X. Chen, Y. Huang, and J. Guan, "Transmit beampattern synthesis for the FDA radar," *IEEE Antennas and Wireless Propagation Letters*, vol. 17, no. 1, pp. 98–101, 2018.

[23] M. Fartookzadeh and S. H. M. Armaki, "Synthesis of serial-fed frequency diverse arrays with periodic triangular frequency-modulated continuous waveform," *IEEE Antennas and Wireless Propagation Letters*, vol. 17, no. 2, pp. 263–266, 2018.

[24] L. Huang, K. D. Gao, Z. M. He, and J. Y. Cai, "Cognitive MIMO frequency diverse array radar with high LPI performance," *International Journal of Antennas and Propagation*, vol. 2016, Article ID 2623617, 11 pages, 2016.

[25] J. Xiong, W. Q. Wang, H. Shao, and H. Chen, "Frequency diverse array transmit beampattern optimization with genetic algorithm," *IEEE Antennas and Wireless Propagation Letters*, vol. 16, pp. 469–472, 2017.

[26] Z. Wang, T. Mu, Y. Song, and Z. Ahmad, "Beamforming of frequency diverse array radar with nonlinear frequency offset based on logistic map," *Progress In Electromagnetics Research*, vol. 64, pp. 55–63, 2018.

[27] Y. Q. Yang, H. Wang, H. Q. Wang, S. Q. Gu, D. L. Xu, and S. L. Quan, "Optimization of sparse frequency diverse array with time-invariant spatial-focusing beampattern," *IEEE Antennas and Wireless Propagation Letters*, vol. 17, no. 2, pp. 351–354, 2018.

[28] Z. Wang, Y. Song, T. Mu, and Z. Ahmad, "A short-range range-angle dependent beampattern synthesis by frequency diverse array," *IEEE Access*, vol. 6, pp. 22664–22669, 2018.

[29] K. Gao, H. Shao, H. Chen, J. Cai, and W. Q. Wang, "Impact of frequency increment errors on frequency diverse array MIMO in adaptive beamforming and target localization," *Digital Signal Processing*, vol. 44, pp. 58–67, 2015.

[30] J. Li, H. Li, and S. Ouyang, "Identifying unambiguous frequency pattern for target localisation using frequency diverse array," *Electronics Letters*, vol. 53, no. 19, pp. 1331–1333, 2017.

[31] W.-Q. Wang and H. Shao, "Range-angle localization of targets by a double-pulse frequency diverse array radar," *IEEE Journal on Selected Topics in Signal Processing*, vol. 8, no. 1, pp. 106–114, 2014.

[32] C. A. Balanis, *Antenna Theory: Analysis and Design*, Wiley, 3rd edition, 2005.

[33] A. Fenn, *Adaptive Antennas and Phased Arrays for Radar and Communications*, Artech House, 2008.

[34] H. L. Van Trees, *Optimum Array Processing*, Wiley, New York, NY, USA, 2002.

[35] P. Stoica and R. Moses, *Spectral Analysis of Signals*, Pearson Prentice-Hall, Upper Saddle River, NJ, USA, 2005.